arXiv:cond-mat/0409779v2 [cond-mat.supr-con] 16 Dec 2004

Ginzburg-Landau Vortex Lattice in Superconductor Films of Finite Thickness

E. H. Brandt
Max-Planck-Institut für Metallforschung, D-70506 Stuttgart, Germany

(Dated: February 2, 2008)

The Ginzburg-Landau equations are solved for ideally periodic vortex lattices in superconducting films of arbitrary thickness in a perpendicular magnetic field. The order parameter, current density, magnetic moment, and the 3-dimensional magnetic field inside and outside the film are obtained in the entire ranges of the applied magnetic field, Ginzburg Landau parameter κ, and film thickness. The superconducting order parameter varies very little near the surface ($\approx 1\%$) and the energy of the film surface is small. The shear modulus c_{66} of the triangular vortex lattice in thin films coincides with the bulk c_{66} taken at large κ. In thin type-I superconductor films with $\kappa < 1/\sqrt{2}$, c_{66} can be positive at low fields and negative at high fields. The magnetization of thin films at small applied fields is enhanced beyond its bulk value $-H_{c1}$ due to the energy of the magnetic stray field.

PACS numbers: 74.25.Qt, 74.78.Bz, 74.78.Db

I. INTRODUCTION

Since Abrikosov's[1] prediction of the flux-line lattice in Type-II superconductors from Ginzburg-Landau (GL) theory, most theoretical work on this vortex lattice in bulk and thin film superconductors considered the situation when the applied magnetic field and the average induction $\bar{B}$ are close to the upper critical field $B_{c2} = \mu_0 H_{c2}$, since analytical solutions may be obtained for this particular case. In the opposite limit of low induction $\bar{B} \ll B_{c2}$, the properties of an isolated vortex and the interaction between vortices are obtained to good approximation from the London theory when the GL parameter κ is not too small, $2\kappa^2 \gg 1$.[1,2,3] The problem of an isolated vortex in thin films was solved analytically within London theory by Pearl[4]; the interaction energy of such Pearl vortices (or pancake vortices[5]) is easily calculated by noting that within London theory the currents and magnetic fields of the vortices superimpose linearly and that the force on a vortex equals the thickness-integrated super-current density at the vortex core times the quantum of flux Φ_0. In thin films with thickness d smaller than the London magnetic penetration depth λ the range of the vortex–vortex interaction is increased to the effective penetration depth $\Lambda = \lambda^2/d$ since the interaction now occurs mainly via the magnetic stray field outside the film.[4,5] Vortices in superconducting films of finite thickness ($d < \lambda$ and $d \geq \lambda$) and in the superconducting half space ($d \gg \lambda$) were calculated from GL theory[6] and London theory.[7,8,9]

At larger reduced induction $b = \bar{B}/B_{c2} > 0.05$ when the London theory does not apply, the properties of the GL vortex lattice have to be computed numerically. A very efficient method[10] uses Fourier series as trial functions for the GL function $|\psi(x,y)|^2$ and magnetic field $B(x,y)$ and minimizes the GL free energy with respect to a finite number of Fourier coefficients. This numerical method was recently improved[11,12] by solving the GL equations iteratively with high precision.

The present paper extends this two-dimensional (2D) method to the 3D problem of a film of arbitrary thickness containing a periodic lattice of GL vortices oriented perpendicular to the film plane. Due to the Fourier ansatz, the magnetic stray field energy is easily accounted for in this method. Moreover, it turns out that the extension from 2D to a 3D problem only slightly increases the required computation time and computer memory, so that high precision can be achieved easily on a Personal Computer. Like in Refs. 11,12, we consider here vortex lattices with arbitrary shape of the unit cell containing one vortex, i.e., our method computes triangular, rectangular, square lattices, etc., and yields also the shear moduli[13] of the equilibrium lattices. The approximate shear modulus c_{66} of the triangular vortex lattice in thin films was computed from GL theory for $b \ll 1$ and $1 - b \ll 1$ in Ref. 14. For early work on films with perpendicular vortex lattice see Refs. 2,3,15,16,17,18,19.

Though we consider here isotropic superconductors, the corresponding results for anisotropic superconductors with principal symmetry axes along x, y, z may be obtained from this isotropic method by scaling the coordinates and introducing an effective GL parameter $\tilde{\kappa}$.[20,21,22] The magnetic field of a vortex inside a uniaxially anisotropic superconductor with surface parallel to the a, c symmetry plane and perpendicular to the vortex line was calculated from anisotropic London theory[13] and compared with experiments in Ref. 23.

The main effect of the flat surface of a superconductor film or half space is the widening of the magnetic field lines of the vortices as they approach the surface. This widening minimizes the sum of the bulk free energy plus the energy of the magnetic stray field outside the superconductor. The resulting magnetic field lines cross the superconductor surface smoothly, see Fig. 1 for the vortex lattice and Figs. 1,2 of Ref. 9 for isolated vortices. One can see that for the *vortex lattice* the field lines at the boundary of the Wigner-Seitz cell are exactly parallel to z, inside and outside the superconductor, and at some distance outside from the surface ($\approx$ half the vortex spacing) the magnetic field becomes uniform and thus the field lines are parallel and equidistant. For the *isolated vortex*, the field lines away from the surface approach radial lines as if they would originate from a point source, a magnetic monopole with strength $2\Phi_0$ situated on the vortex core at a distance 1.27λ below the surface.[9]

In Ref. 6 the widening of the field lines inside the superconductor was missed, but some modification of the superconductor order parameter near the surface was calculated from GL theory. Below we obtain that the correct modification of $|\psi|^2$ is very small: the vortex core, visualized as contour lines of $|\psi(x,y,z)|^2$, widens near the surface by only a few percent.

The outline of this paper is as follows. In Sct. 2 the solution method is outlined. Section 3 presents a selection of results for thin and thick films: Magnetic field lines, profiles of the order parameter and magnetic field, the variances of the periodic order parameter and magnetic field inside and outside the film, surface energy and stray-field energy, and shear modulus of the triangular vortex lattice in the film. A summary is given in Sct. 4.

II. SOLUTION METHOD

The properties of the vortex lattice within GL theory are calculated by minimizing the GL free energy of the superconductor with respect to the complex GL function $\psi(\mathbf{r})$ and to the vector potential $\mathbf{A}(\mathbf{r})$ of the local magnetic induction $\mathbf{B}(\mathbf{r}) = \nabla \times \mathbf{A}$. In the usual reduced units[1,2] (length λ, magnetic induction $\sqrt{2}\mu_0 H_c$, energy density $\mu_0 H_c^2$, where $H_c = H_{c2}/(\sqrt{2}\kappa)$ is the thermodynamic critical field) the spatially averaged free energy density F of the GL theory referred to the Meissner state ($\psi = 1$, $\mathbf{B} = 0$) within the superconductor reads

$$F = \left\langle \frac{(1-|\psi|^2)^2}{2} + \left| \left(\frac{\nabla}{i\kappa} - \mathbf{A} \right) \psi \right|^2 + \mathbf{B}^2 \right\rangle . \quad (1)$$

Here $\langle \ldots \rangle = (1/V) \int_V d^3r \ldots$ means spatial averaging over the superconductor with volume V. Introducing the supervelocity $\mathbf{Q}(\mathbf{r}) = \mathbf{A} - \nabla\varphi/\kappa$ and the magnitude $f(\mathbf{r}) = |\psi|$ of $\psi(\mathbf{r}) = f(\mathbf{r}) \exp[i\varphi(\mathbf{r})]$ one may write F as a functional of the real and gauge-invariant functions f and $\mathbf{Q}$,

$$F = \left\langle \frac{(1-f^2)^2}{2} + \frac{(\nabla f)^2}{\kappa^2} + f^2 Q^2 + (\nabla \times \mathbf{Q})^2 \right\rangle . \quad (2)$$

In the presence of vortices $\mathbf{Q}(\mathbf{r})$ has to be chosen such that $\nabla \times \mathbf{Q}$ has the appropriate singularities along the vortex cores, where f vanishes. By minimizing this F with respect to ψ, $\mathbf{A}$ or f, $\mathbf{Q}$, one obtains the GL equations together with the appropriate boundary conditions. For the superconducting film considered here, one has to add the energy of the magnetic stray field outside the film, which makes $\mathbf{B}$ continuous at the film surface, see below.

The 3D solution of the GL equations for an infinitely large, thick or thin film with periodic lattice of vortices perpendicular to the film plane, can be obtained numerically by a modification of the 2D method developed in Refs. 11,12. This is possible since in any plane $z = \text{const}$ parallel to the film the solutions for the ideal vortex lattice are still periodic. Actually this periodicity applies even to tilted and arbitrarily curved vortex lines, and to anisotropic superconductors, which may be computed by a similar method. These more complex problems will be considered in future work.

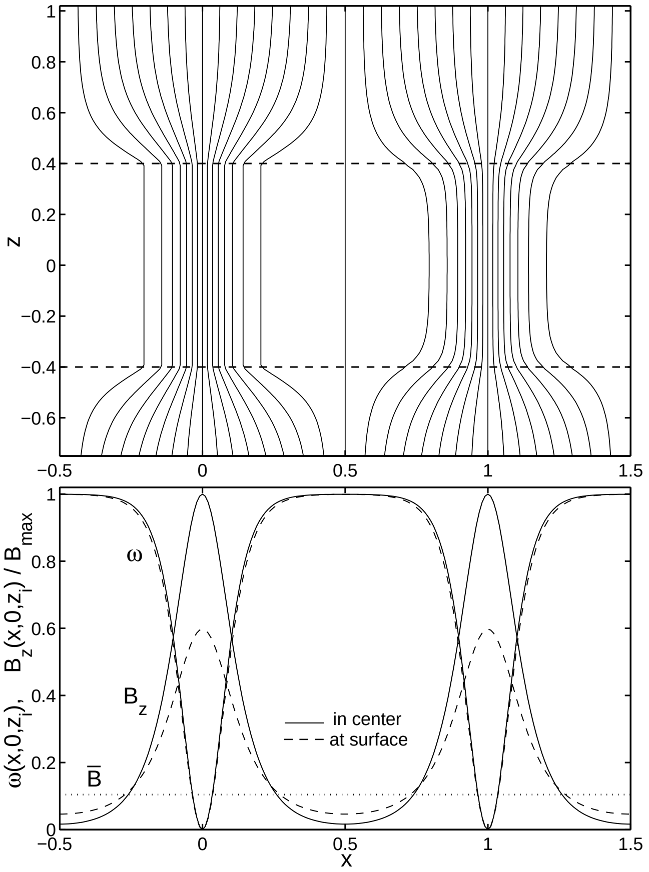

FIG. 1: Magnetic field lines (top) and profiles of order parameter $|\psi|^2 = \omega(x, 0, z_i)$ and magnetic field $B_z(x, 0, z_i)$ (bottom) for a superconductor film calculated from Ginzburg-Landau theory for the triangular vortex lattice. Shown is the example $b = \bar{B}/B_{c2} = 0.04$, $\kappa = 1.4$, triangular lattice with vortex spacing (unit length) $x_1 = 3^{-1/4}(2\Phi_0/\bar{B})^{1/2} = 5x_1(B_{c2}) \approx 10\lambda$, film thickness $d = 0.8x_1 \approx 8\lambda$. Top: The left half shows the field lines that would apply if the field in the film would not change near the surfaces $z = \pm d/2$ marked by dashed lines. The right half shows the correct solution. The density of the depicted field lines is proportional to the local induction $|\mathbf{B}|$, see Appendix A and Fig. 2. Bottom: The solid lines show ω and B in the center of the film ($z = 0$) and the dashed lines at the film surfaces. The average induction $\bar{B}$ is marked as a dotted line.

For the present problem of straight vortices along z one may choose a general ansatz for the magnitude of the GL function $f(x, y, z) = |\psi(x, y, z)|$ in form of the following

3D Fourier series for the smooth function f^2:

$$\omega(\mathbf{r}) = f^2 = \sum_{\mathbf{K}} a_{\mathbf{K}} (1 - \cos \mathbf{K}_\perp \mathbf{r}_\perp) \cos K_z z \,. \qquad (3)$$

Here $\mathbf{r} = (x, y, z)$, $\mathbf{r}_\perp = (x, y)$, $\mathbf{K} = (K_x, K_y, K_z)$, $\mathbf{K}_\perp = (K_x, K_y)$. In all sums here and below the term $\mathbf{K}_\perp = 0$ is excluded. For vortex positions $\mathbf{R} = \mathbf{R}_{mn} = (mx_1 + nx_2,\, ny_2)$ the reciprocal lattice vectors are $\mathbf{K}_\perp = \mathbf{K}_{mn} = (2\pi/S)(my_2,\, nx_1 + mx_2)$ with $S = x_1 y_2 = \Phi_0/\bar{B}$ the unit cell area and $m = 0, \pm 1, \pm 2, \dots$, $n = 0, \pm 1, \pm 2, \dots$. The z-component of $\mathbf{K}$ is chosen as $K_z = (2\pi/d)l$ with $l = 0,\ 1,\ 2,\ \dots$ and d the film thickness. This ansatz guarantees that $f(\mathbf{R}, z) = 0$ at the (straight) vortex cores and that at the two surfaces of the film $z = \pm d/2$ one has $\partial(f^2)/\partial z = 0$, as it follows from the variation of the GL free energy functional (2). If only the term $K_z = 0$ is kept, the ansatz (3) reduces to that for the 2D vortex lattice in Ref. 1. Formally, the 3D Fourier series (3) may also be expressed as a 2D Fourier series with z dependent coefficients $a_{\mathbf{K}_\perp}(z) = \sum_{K_z} a_{\mathbf{K}} \cos K_z z$.

For the supervelocity $\mathbf{Q}$ and magnetic induction $\mathbf{B} = \nabla \times \mathbf{Q}$ inside the film we chose the general ansatz

$$\begin{aligned} \mathbf{Q}(\mathbf{r}) &= \mathbf{Q}_A(\mathbf{r}_\perp) + \mathbf{q}(\mathbf{r}), \\ \mathbf{B}(\mathbf{r}) &= \bar{B}\hat{\mathbf{z}} + \mathbf{b}(\mathbf{r}), \quad \langle \mathbf{b}(\mathbf{r}) \rangle = 0, \\ \mathbf{b}(\mathbf{r}) &= \nabla \times \mathbf{q}(\mathbf{r}) \,. \end{aligned} \qquad (4)$$

Here $\mathbf{Q}_A(x, y)$ is the supervelocity of the Abrikosov B_{c2} solution, which satisfies

$$\nabla \times \mathbf{Q}_A = \Big[\bar{B} - \Phi_0 \sum_{\mathbf{R}} \delta_2(\mathbf{r}_\perp - \mathbf{R}) \Big] \hat{\mathbf{z}} \,, \qquad (5)$$

where $\delta_2(\mathbf{r}_\perp) = \delta(x)\delta(y)$ is the 2D delta function and Φ_0 the quantum of flux, $\Phi_0 = 2\pi/\kappa$ in reduced units. Formula (5) shows that $\mathbf{Q}_A$ is the velocity field of a lattice of ideal vortex lines but with zero average rotation. Near each vortex center one has $\mathbf{Q}_A(\mathbf{r}_\perp) \approx \hat{\mathbf{z}} \times \mathbf{r}'_\perp/(2\kappa r'^2_\perp)$ and $f(\mathbf{r})^2 \propto r'^2_\perp$ with $\mathbf{r}'_\perp = \mathbf{r}_\perp - \mathbf{R}$. $\mathbf{Q}_A(\mathbf{r}_\perp)$ may be expressed as a slowly converging Fourier series by integrating (5) using $\mathrm{div}\mathbf{Q} = \mathrm{div}\mathbf{Q}_A = 0$. It is, however, more convenient to take $\mathbf{Q}_A$ from the exact relation

$$\mathbf{Q}_A(\mathbf{r}_\perp) = \frac{\nabla \omega_A \times \hat{\mathbf{z}}}{2\,\kappa\,\omega_A} \,, \qquad (6)$$

where $\omega_A(x, y) = f(x, y)^2$ is the Abrikosov B_{c2} solution given by a rapidly converging series of type (3) with z-independent coefficients

$$a^A_{\mathbf{K}_\perp} = -(-1)^{m+mn+n} \exp[-K^2_{mn} S/(8\pi)] \qquad (7)$$

for general vortex-lattice symmetry, and $a^A_{\mathbf{K}_\perp} = -(-1)^\nu \exp(-\pi\nu/\sqrt{3})$ $(\nu = m^2 + mn + n^2)$ for the triangular lattice. The ω_A from (7) is normalized to $\langle \omega_A(x, y) \rangle = 1$; this yields the strange relation $\sum'_{\mathbf{K}_\perp} a^A_{\mathbf{K}_\perp} = 1$ for any lattice symmetry. Another strange property of the Abrikosov solution (7) is that $(\nabla\omega_A/\omega_A)^2 - \nabla^2\omega_A/\omega_A = 4\pi/S = \mathrm{const}$, although both terms diverge at the vortex positions; this relation follows from (5) and (6) using $\bar{B} = \Phi_0/S = 2\pi/(\kappa S)$. The useful formula (6) may be proven via the complex B_{c2} solution $\psi_A(x, y)$; it means that near B_{c2} the second and third terms in the F, Eq. (2), are equal.

The general ansatz for $\mathbf{q}(\mathbf{r}) = (q_x, q_y, q_z)$ is a Fourier series for all three components, satisfying $\nabla \times \mathbf{q} = \mathbf{b}$. For simplicity here I shall assume $q_z = 0$, which means planar supercurrents. In the considered case of vortices perpendicular to the film plane this is an excellent approximation, which is exact in the limit of small induction and probably also at large inductions $\bar{B} \approx B_{c2}$, and it is exact for thin films. I further assume $\nabla \cdot \mathbf{Q} = 0$, which is exact in several special cases (e.g. for $\bar{B} \ll B_{c2}$ and $\bar{B} \approx B_{c2}$) and is possibly exact even in the general case, though I did not find a proof for this. Note also that within the circular cell approximation[1,2] both assumptions are satisifed. With these two assumptions $\mathbf{q}$ is fully determined by the z-component of $\mathbf{b} = (\mathbf{b}_\perp, b_z)$:

$$\begin{aligned} b_z(\mathbf{r}) &= \sum_{\mathbf{K}} b_{\mathbf{K}} \cos \mathbf{K}_\perp \mathbf{r}_\perp \cos K_z z \,, \\ \mathbf{b}_\perp(\mathbf{r}) &= \sum_{\mathbf{K}} b_{\mathbf{K}} \frac{\mathbf{K}_\perp K_z}{K^2_\perp} \sin \mathbf{K}_\perp \mathbf{r}_\perp \sin K_z z \\ \mathbf{q}(\mathbf{r}) &= \sum_{\mathbf{K}} b_{\mathbf{K}} \frac{\hat{\mathbf{z}} \times \mathbf{K}_\perp}{K^2_\perp} \sin \mathbf{K}_\perp \mathbf{r}_\perp \cos K_z z \,, \end{aligned} \qquad (8)$$

with $K_\perp = |\mathbf{K}_\perp|$. Formally, these 3D Fourier series (8) may also be expressed as 2D Fourier series with z dependent coefficients $b_{\mathbf{K}_\perp}(z) = \sum_{K_z} b_{\mathbf{K}} \cos K_z z$ and their derivatives $b'_{\mathbf{K}_\perp}(z)$. The solution is thus completely determined by the two infinite sets of scalar Fourier coefficients $a_{\mathbf{K}}$ and $b_{\mathbf{K}}$, which are obtained by minimizing the total free energy with respect to these coefficients for given parameters κ and $\bar{B}$ and film thickness d. For the computation I shall use a large but finite number of $a_{\mathbf{K}}$ and $b_{\mathbf{K}}$ in the sense of a Ritz variational method.

The total free energy F_{tot} per unit volume of the infinite film is the sum of the GL free energy, Eq. (2), and the stray-field energy F_{stray}. In reduced units and referred to the state where $\psi = 0$ and $\mathbf{B}(\mathbf{r}) = \bar{B}\hat{\mathbf{z}} = \mu_0 H_a \hat{\mathbf{z}}$ one has with $g = (\nabla f)^2/\kappa^2 = (\nabla\omega)^2/(4\kappa^2\omega)$:

$$\begin{aligned} F_{\mathrm{tot}} &= \langle -\omega + \tfrac{1}{2}\omega^2 + g + \omega Q^2 + b^2 \rangle + \frac{F_{\mathrm{stray}}}{d}, \\ F_{\mathrm{stray}} &= 2 \int_{d/2}^{\infty} \langle\, \mathbf{B}(\mathbf{r})^2 - \bar{B}^2 \,\rangle_{x,y} \, dz. \end{aligned} \qquad (9)$$

The factor of 2 comes from the two half spaces above and below the film, which contribute equally to F_{stray}. The stray field $\mathbf{B}(x, y, z > d/2)$ with constant planar average $\langle \mathbf{B}(x, y, z) \rangle_{x,y} = \bar{B}\hat{\mathbf{z}}$ is determined by the Laplace equation $\nabla^2 \mathbf{B} = 0$ (since $\nabla \cdot \mathbf{B} = 0$ and $\nabla \times \mathbf{B} = 0$ in vacuum) and by its perpendicular component at the film surface $z = d/2$, since B_z has to be continuous across this surface. This yields with (8) the stray field:

$$B_z(x, y, z \geq d/2) =$$

$$\sum_{\mathbf{K}_\perp} b^s_{\mathbf{K}_\perp}\cos(\mathbf{K}_\perp\mathbf{r}_\perp)\exp[-K_\perp(z-d/2)]+\bar{B}\,,$$
$$\mathbf{B}_\perp(x,y,z\geq d/2)=$$
$$\sum_{\mathbf{K}_\perp} b^s_{\mathbf{K}_\perp}\frac{\mathbf{K}_\perp}{K_\perp}\sin(\mathbf{K}_\perp\mathbf{r}_\perp)\exp[-K_\perp(z-d/2)]\,,$$
$$b^s_{\mathbf{K}_\perp}=b_{\mathbf{K}_\perp}(z=d/2)=\sum_l b_{\mathbf{K}}\cos(\pi l)\,. \tag{10}$$

($l=0,1,2,\ldots$). For spatial averaging we shall need the orthonormality relations valid for $\mathbf{K}_\perp\neq 0$:

$$\begin{aligned}\langle\cos(\mathbf{K}_\perp\mathbf{r}_\perp)\cos(\mathbf{K'}_\perp\mathbf{r}_\perp)\rangle_{x,y} &= \\ \langle\sin(\mathbf{K}_\perp\mathbf{r}_\perp)\sin(\mathbf{K'}_\perp\mathbf{r}_\perp)\rangle_{x,y} &= \frac{1}{2}\,\delta_{\mathbf{K}_\perp\mathbf{K'}_\perp}\,,\end{aligned} \tag{11}$$

$$\begin{aligned}\left\langle\cos\frac{2\pi lz}{d}\cos\frac{2\pi l'z}{d}\right\rangle_z &= \delta_{l,l'}\frac{1+\delta_{l,0}}{2}\,,\\ \left\langle\sin\frac{2\pi lz}{d}\sin\frac{2\pi l'z}{d}\right\rangle_z &= \delta_{l,l'}\frac{1-\delta_{l,0}}{2}\,.\end{aligned} \tag{12}$$

Averaging the squared stray field over x and y and using (11), (12) one obtains terms $(b^s_{\mathbf{K}_\perp})^2\exp[-2K_\perp(z-d/2)]$, and thus $F_{\rm stray}$ in Eq. (9) becomes

$$F_{\rm stray}=\sum_{\mathbf{K}_\perp}\frac{(\,b^s_{\mathbf{K}_\perp})^2}{K_\perp}\,. \tag{13}$$

The Fourier coefficients $a_\mathbf{K}$ and $b_\mathbf{K}$ may be computed by iterating appropriate GL equations as shown in Ref. 11,12. Minimizing F, Eq. (2), with respect to f and $\mathbf{Q}$ yields the two GL equations for bulk superconductors

$$\kappa^{-2}\nabla^2 f = -f+f^3+fQ^2\,, \tag{14}$$
$$\mathbf{j}=\nabla\times\mathbf{B}=\nabla\times\nabla\times\mathbf{Q}=-f^2\mathbf{Q}\,. \tag{15}$$

The first GL equation (14) applies also to our film; the second GL equation (15), too, but when it is written as an equation for the $b_\mathbf{K}$ it has to be supplemented by a stray-field term $\sim\delta F_{\rm stray}/\delta\mathbf{Q}$ on its r.h.s., which originates from the boundary condition for $\mathbf{B}$. A possible iteration equation for the $a_\mathbf{K}$ is obtained from (14) using the relation $2f\nabla^2 f=\nabla^2\omega-(\nabla\omega)^2/(2\omega)$ to give

$$\nabla^2\omega = 2\kappa^2\,(-\omega+\omega^2+\omega Q^2+g\,) \tag{16}$$

with $g=(\nabla\omega)^2/(4\kappa^2\omega)$ as above. Note that ∇ here means the 3D Nabla operator, while the similar Eq. (9) of Ref. 11 is 2D. To obtain better convergence of the iteration I subtract a term $2\kappa^2\omega$ on both sides of (16), such that K^2 is replaced by $K^2+2\kappa^2$; this choice yields fastest convergence. Using the ansatz (3) and the orthonormalities (11), (12) we then obtain an iteration equation for the $a_\mathbf{K}$:

$$a_\mathbf{K}:=\frac{\langle(\omega^2-2\omega+\omega Q^2+g)\,\cos\mathbf{K}_\perp\mathbf{r}_\perp\cos K_z z\rangle}{\frac{1}{4}\,(\delta_{K_z,0}+1)\,(K^2/2\kappa^2+1)}\,, \tag{17}$$

where $\langle\ldots\rangle$ averages over x,y,z. In particular, if ω and $\mathbf{Q}$ do not depend on z, Eq. (17) reduces to Eq. (11) of Ref. 11 and yields $a_\mathbf{K}=0$ for all $K_z\neq 0$. Other forms of iteration equations for the $a_\mathbf{K}$ are possible, e.g. one containing in the denominator $K_\perp^2$ instead of K^2, but one should choose that which yields fastest convergence of the iteration. In general, the iteration of any equation for some parameter a given in the original form $a:=F(a)$ may be made more stable or faster converging by rewriting it in the form $a:=(1-c)a+cF(a)$ with some constant $c\leq 1$ (or even $c>1$ in some cases).

The convergence is accelerated by alternating the iteration step (17) with an iteration step that changes only the amplitude of ω but not its shape. Namely, from $\partial F_{\rm tot}/\partial\langle\omega\rangle=0$ we obtain

$$a_\mathbf{K}:=a_\mathbf{K}\frac{\langle\omega-g-\omega Q^2\rangle}{\langle\omega^2\rangle}\,. \tag{18}$$

Similarly, an iteration equation for the $b_\mathbf{K}$ is obtained from the equation $\partial F_{\rm tot}/\partial b_\mathbf{K}=0$ by reordering the terms appropriately. From Eq. (8)-(13) one has

$$\frac{\partial\langle b^2\rangle}{\partial b_\mathbf{K}} = b_\mathbf{K}\frac{(1+\delta_{l,0})K_\perp^2+(1-\delta_{l,0})K_z^2}{2K_\perp^2} \tag{19}$$
$$\frac{\partial\langle\omega Q^2\rangle}{\partial b_\mathbf{K}} = \frac{2P_\mathbf{K}}{K_\perp^2} \tag{20}$$
$$\frac{1}{d}\frac{\partial F_{\rm stray}}{\partial b_\mathbf{K}} = b^s_{\mathbf{K}_\perp}\frac{2\cos(\pi l)}{d\,K_\perp} \tag{21}$$

with $b^s_{\mathbf{K}_\perp}$ from Eq. (10) and

$$P_\mathbf{K}=\langle\,\omega(Q_yK_x-Q_xK_y)\sin\mathbf{K}_\perp\mathbf{r}_\perp\cos K_z z\,\rangle\,. \tag{22}$$

Equating the sum of the terms (19)–(21) to zero and adding and subtracting an appropriate term $c\langle\omega\rangle b_\mathbf{K}$ that improves the convergence (with some constant $c\approx 1$ or larger), one obtains an iteration equation for the $b_\mathbf{K}$:

$$b_\mathbf{K}:=\frac{-2P_\mathbf{K}+c\langle\omega\rangle\,b_\mathbf{K}-\frac{2}{d}K_\perp b^s_{\mathbf{K}_\perp}\cos(\pi l)}{\delta_{l,0}K_\perp^2+\frac{1}{2}\,(1-\delta_{l,0})K^2+c\langle\omega\rangle}\,. \tag{23}$$

The solutions $\omega(\mathbf{r})$, $\mathbf{B}(\mathbf{r})$, and $\mathbf{Q}(\mathbf{r})$ are obtained iteratively by first finding the 2D solution as in Ref. 11,12, keeping only the terms with $K_z=0$ and starting, e.g., with $a_\mathbf{K}=(1-\bar{B}/B_{c2})\,a^A_{\mathbf{K}_\perp}$ and $b_\mathbf{K}=0$ and then iterating the three equations (17), (18), (23) by turns a few times; after this, the 3D solution is obtained by continuing this iteration with the terms for all K_z included until the coefficients $a_\mathbf{K}$ and $b_\mathbf{K}$ do not change any more. With the empirical choice $c\approx 3+(0.4+60b^2)\kappa^2 x_1/d$ this iteration is stable for all b, κ, and d and the free energy decreases smoothly until it becomes stationary (with accuracy 10^{-14}) after $25\ldots50$ iteration steps.

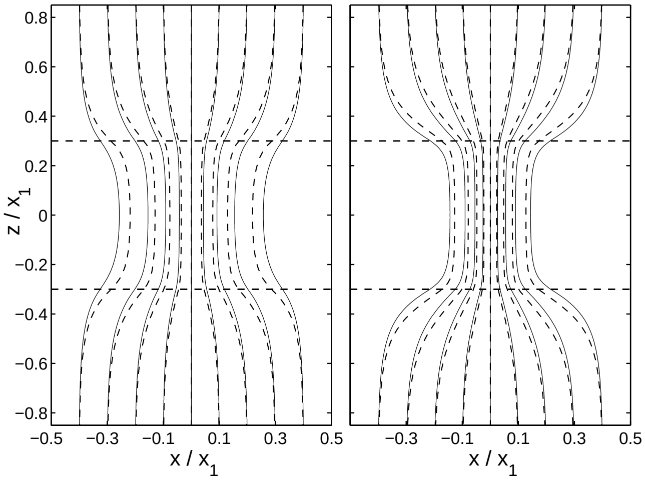

FIG. 2: Comparison of the magnetic field lines plotted either as stream lines (solid lines) that flow along the exact direction of the magnetic field but do not show the correct 2D flux density, or as contour lines (dashed lines, see Appendix A) that show the correct flux density but have only approximately the orientation the magnetic field. Shown are the examples $b = 0.04$, triangular lattice, with (right plot) $\kappa = 2$, $d = 0.6x_1 \approx 4\lambda$ and (left plot) $\kappa = 1$, $d = 0.6x_1 \approx 8\lambda$. The horizontal dashed lines indicate the film surfaces $z = \pm d/2$.

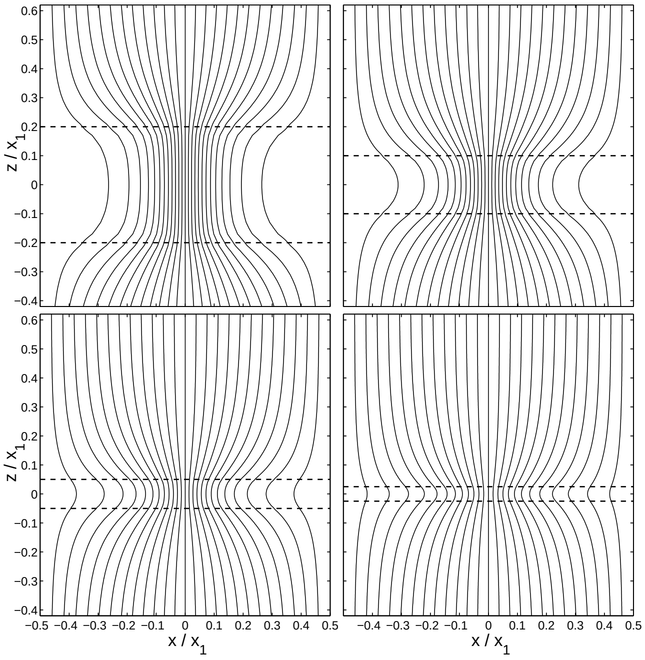

FIG. 3: The magnetic field lines of the vortex lattice in films of various thicknesses $d/\lambda \approx 4$, 2, 1, 0.5, corresponding to $d/x_1 = 0.4$, 0.2, 0.1, 0.05, for $b = 0.04$ and $\kappa = 1.4$. Depicted is the field in the plane $y = 0$ in one lattice cell. The film surfaces are marked by two dashed lines. The field lines of an isolated vortex in such films are shown in Fig. 2 of Ref. 9.

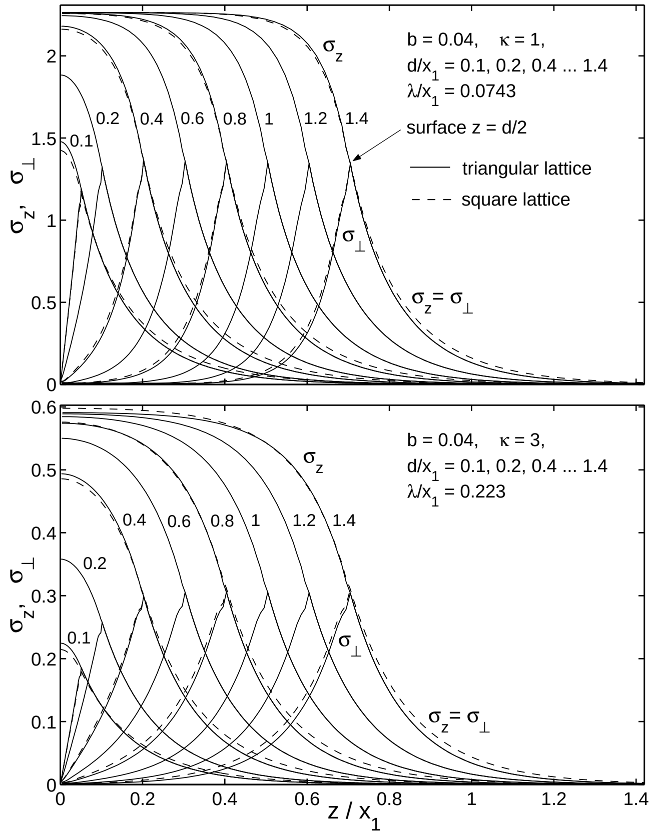

FIG. 4: The variances of the longitudinal and transverse components of the magnetic induction, $\sigma_z(z)$ and $\sigma_\perp(z)$, defined by Eqs. (24), (25), plotted versus z/x_1 (x_1 = vortex spacing) at reduced induction $b = 0.04$ for films of various thicknesses $d/x_1 = 0.1$, 0.2, 0.4, 0.6, 0.8, 1, 1.2, and 1.4. Top: For $\kappa = 1$, yielding $\lambda/x_1 = 0.0743$. Bottom: For $\kappa = 3$, thus $\lambda/x_1 = 0.223$. While $\sigma_z(z)$ decreases monotonically with increasing z, $\sigma_\perp(z)$ has a sharp peak at the film surface $z = d/2$. Outside the film ($|z| \geq d/2$) one has $\sigma_z(z) = \sigma_\perp(z)$.

III. SOME RESULTS

A. Magnetic field and order parameter

Figure 1 shows one example for the resulting magnetic field lines and some cross sections of $\omega(x, y, z)$ and $\mathbf{B}(x, y, z)$ along x in the plane $y = 0$ at $z = 0$ (center plane of the film) and $z = d/2$ (film surface), for a film of finite thickness $d = 0.8x_1 \approx 8\lambda$ at reduced induction $b = \bar{B}/B_{c2} = 0.04$ and GL parameter $\kappa = 1.4$, yielding for the triangular vortex lattice a vortex spacing of $x_1(B) = 5x_1(B_{c2}) = 1.25d \approx 10\lambda$. The left half of Fig. 1 shows the field lines that result if the unchanged 2D bulk solutions for $B(x, y)$ and $\omega(x, y)$ are assumed inside the film. The right half shows the correct solution, exhibiting smooth field lines across the film surface, and a very weak widening of the vortex core near the surface.

Figure 2 shows the magnetic field lines for a film with

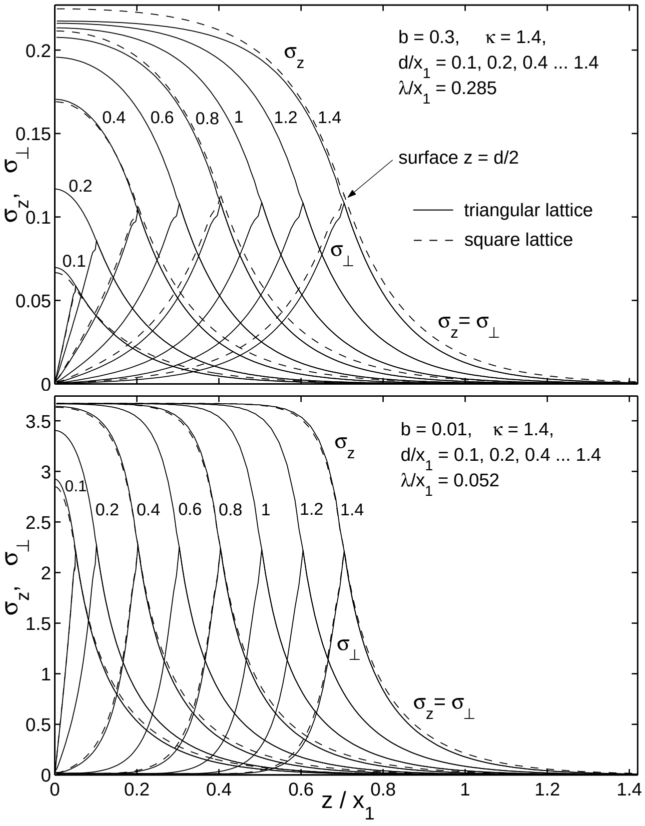

FIG. 5: As Fig. 4 but for $\kappa = 1.4$ and two b values. Top: Large $b = 0.3$, yielding $\lambda/x_1 = 0.285$. Bottom: Low $b = 0.01$, thus $\lambda/x_1 = 0.0520$.

thickness $d = 0.6x_1$ at $b = 0.04$ for $\kappa = 2$ ($d \approx 4\lambda$, left) and $\kappa = 1$ ($d \approx 8\lambda$, right), triangular lattice. The solid lines are the stream lines of $\mathbf{B}(x, 0, z) = (B_x, 0, B_z)$; they have the correct slope of $\mathbf{B}$ and start at equidistant points far away from the film surface, where $\mathbf{B} = \mathbf{B}_a = (0, 0, \bar{B})$ = constant (in infinitely extended films the average induction $\bar{\mathbf{B}}$ equals the applied induction $\mathbf{B}_a$ outside and inside the film), but their 1D density is not proportional to the 2D flux density $B = |\mathbf{B}|$. The dashed lines in Fig. 2 are field lines that have approximately the slope of $\mathbf{B}(x, 0, z)$ and have a density proportional to B, see Appendix A. This type of field lines is depicted also in Figs. 1 and 3.

In Fig. 3 the magnetic field lines are shown for films of various thicknesses $d/x_1 = 0.4, 0.2, 0.1, 0.05$ for $b = 0.04$ and $\kappa = 1.4$ as in Fig. 1, where $d/x_1 = 0.8$. These thicknesses correspond to $d/\lambda \approx 4, 2, 1, 0.5$ (and 0.25 in Fig. 1). At low inductions $b \ll \kappa^{-2}$ and not too small $\kappa > 5$, these field patterns may also be obtained by linear superposition of the fields of isolated London vortices given by Eqs. (5)-(9) of Ref. 9, with appropriately cut-off vortex core introduced to consider the finite coherence length ξ. This superposition also applies to nonperiodic vortex arrangements.

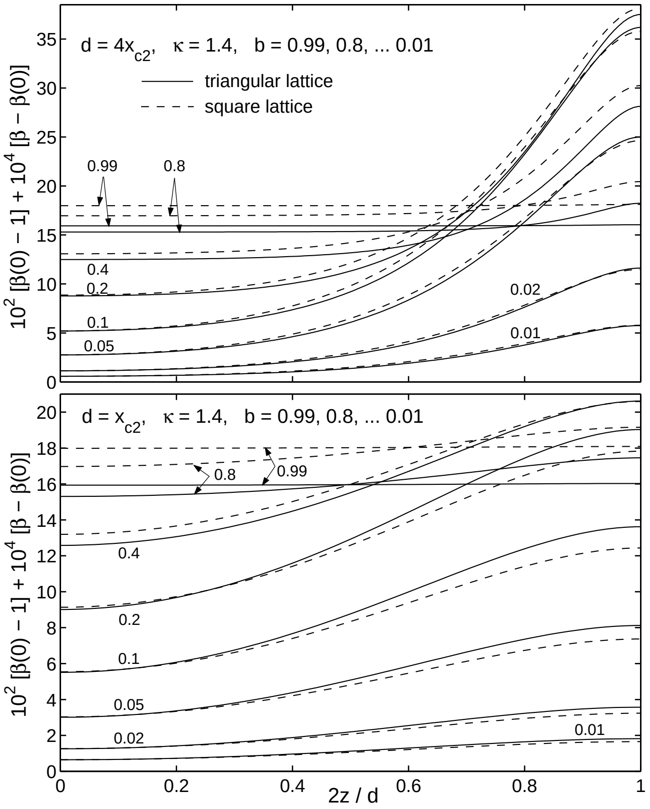

FIG. 6: The spatial variance (Abrikosov parameter) $\beta(z) = \langle \omega^2 \rangle_{x,y} / \langle \omega \rangle_{x,y}^2$, of the order parameter $\omega(x, y, z) = |\psi(x, y, z)|^2$, plotted as $10^4[\beta(z) - \beta(0)] + 100[\beta(0) - 1]$ versus $z/(d/2)$ for several reduced inductions $b = 0.99$, 0.8, 0.4, 0.2, 0.1, 0.05, 0.02, and 0.01 for $\kappa = 1.4$ and for both triangular (solid lines) and square (dashed lines) vortex lattices. Top: Thick film with $d = 4x_{c2}$. Bottom: Thinner film with $d = x_{c2}$. Here $x_{c2} = x_1\sqrt{b} \approx 2.7\xi$ is the vortex spacing at $\bar{B} = B_{c2}$. The extremely small variation of $\beta(z)$ is enlarged by plotting $10^4 \times [\beta(z) - \beta(0)]$. Adding the constant $10^2[\beta(0) - 1]$ allows to identify (at $z = 0$) the bulk Abrikosov values $\beta(0) \approx \beta_A = 1.1596$ (1.8034) occurring for the triangular (square) lattice in thick films when $b \to 1$.

B. Variance of the magnetic induction

Figures 4 and 5 show the two relative variances σ_z and $\sigma_\perp$ of the magnetic induction defined here as

$$\sigma_z(z) = \langle [B_z(x, y, z) - \bar{B}]^2 \rangle_{x,y}^{1/2} / \bar{B} \qquad (24)$$

$$\sigma_\perp(z) = \langle B_x(x, y, z)^2 + B_y(x, y, z)^2 \rangle_{x,y}^{1/2} / \bar{B}\,. \qquad (25)$$

These measures of the relative variation of the periodic induction depend on z: Deep inside thick films, $\sigma_z(z)$ reduces to the variance of the 2D vortex lattice in the bulk, σ_{bulk}, computed, e.g., in Ref. 12 as function of b and κ, and one has $\sigma_\perp = 0$ since $\mathbf{B} \| \hat{\mathbf{z}}$ for the considered case. As one approaches the surface from inside the film, $\sigma_z(z)$ decreases and $\sigma_\perp(z)$ increases until they coincide at the surface $z = d/2$. Outside the superconductor one

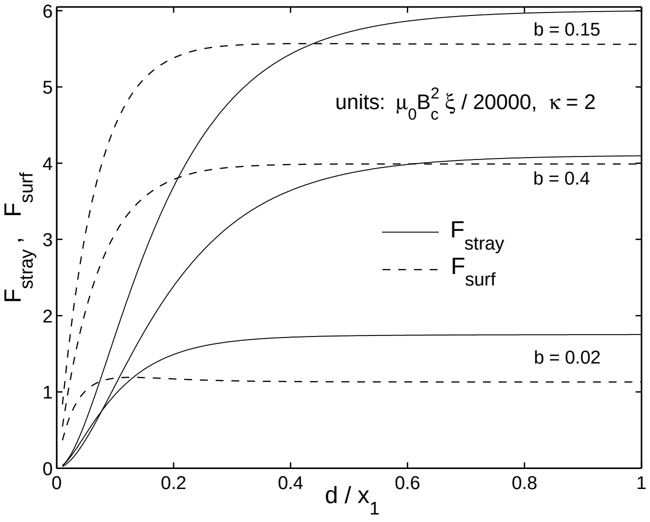

FIG. 7: The energy $F_{\rm stray}$ of the magnetic stray field (solid lines) and the surface energy $F_{\rm surf}$ of the film (dashed lines) plotted versus the film thickness d for $\kappa = 2$ and $b = 0.02$, 0.15, and 0.4, see text. These energies per unit area are plotted in units $\mu_0 H_c^2 \xi/20000$ to enlarge them to order of unity and show their close coincidence at large b.

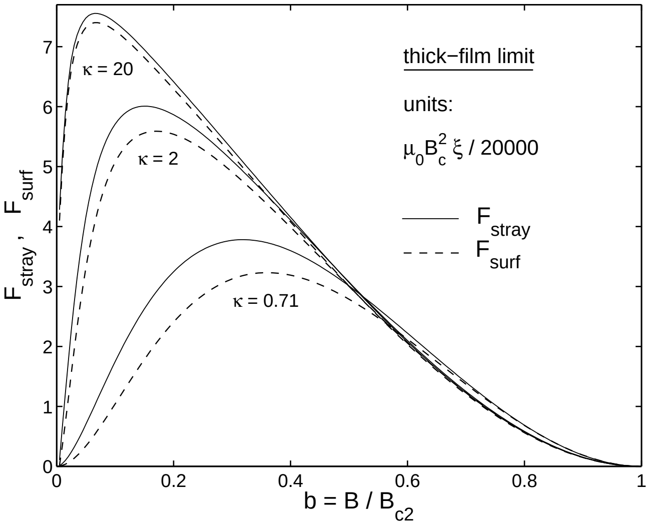

FIG. 8: The thick-film limits of the stray-field energy $F_{\rm stray}$ (solid lines) and the surface energy $F_{\rm surf}$ (dashed lines) plotted versus the reduced induction b for $\kappa = 0.71$, 2, and 20 in units $\mu_0 H_c^2 \xi / 2 \cdot 10^4$.

has exactly

$$\sigma_z^2(z \ge d/2) = \sigma_\perp^2(z \ge d/2)$$
$$= \frac{1}{2\bar B^2} \sum_{\mathbf{K}_\perp} (\, b^s_{\mathbf{K}_\perp})^2 \exp[-2K_\perp(z - d/2)]\,. \qquad (26)$$

This follows from Eqs. (10) for the magnetic stray field. At large $|z| - d/2 \gg x_1/(2\pi)$, the variance decreases exponentially with z, $\sigma_z = \sigma_\perp \propto \exp(-K_{10}|z|)$, where $K_{10} \approx 2\pi/x_1$ is the shortest reciprocal lattice vector of the vortex lattice defined below Eq. (3). Thus, $\sigma_z(z)$ decreases monotonically from its bulk value $\sigma_{\rm bulk}$ inside a thick film to zero far away from the film, reaching at the surface approximately half its bulk value (for thick films). In contrast to this, the transverse variance $\sigma_\perp(z)$ increases from zero at $z = 0$ and reaches a sharp cusp-shaped maximum at the surface, where it joins $\sigma_z(z)$ and then decreases again to zero away from the film. For large $\kappa \ge 2$ and $d/x_1 \ge 0.7$ these curves are approximately symmetric,

$$\begin{aligned}\sigma_z(|z| < d/2) &= \sigma_{\rm bulk} - \sigma_z(d - |z|)\\ \sigma_\perp(|z| < d/2) &\approx \sigma_z(d - |z|)\\ \sigma_\perp(d/2) = \sigma_z(d/2) &\approx \sigma_{\rm bulk}/2\;. \end{aligned} \qquad (27)$$

This is so since for $\lambda \gg x_1/2\pi$ the outer and inner magnetic stray fields are symmetric.

Shown in Figs. (4) and (5) are both variances for various values of b and κ for 8 film thicknesses $d/x_1 = 0.1$, 0.2, 0.4, 0.6, 0.8, 1, 1.2, and 1.4 for the triangular vortex lattice (solid lines) and for $d/x_1 = 0.1$, 0.4, 0.8, and 1.2 for the square vortex lattice (dashed lines). The variances for these two lattice symmetries are almost identical.

C. Variance of the order parameter

Figure 6 shows the variance of the order parameter $\omega(x,y,z) = |\psi(x,y,z)|^2$ inside films with periodic vortex lattice,

$$\beta(z) = \frac{\langle\, \omega(x,y,z)^2 \,\rangle_{x,y}}{\langle\, \omega(x,y,z) \,\rangle_{x,y}^2}. \qquad (28)$$

At large reduced inductions $b = \bar B/B_{c2} \to 1$ in the middle of thick films $\beta(z)$ coincides with the Abrikosov parameter $\beta_A = 1.15960$ for the triangular vortex lattice and $\beta_A = 1.18034$ for the square lattice. At low inductions $b \to 0$ one has $\beta \to 1$ since the order parameter ω is constant except in the small vortex cores. Figure 6 shows that $\beta(z)$, and thus the shape of $\omega(x,y,z)$, changes very little with z. For films of thickness $d > 4x_{c2}$, one has constant bulk β in a central region around $z = 0$, and as z approaches the surface of the film, $\beta(z)$ increases by at most a factor of 1.0033 within a layer of thickness $\approx x_{c2}$. Here $x_{c2} = x_1(B_{c2}) = x_1\sqrt{b}$ is the vortex distance at $\bar B = B_{c2}$. One has $x_{c2}^2 = (4\pi/\sqrt{3})\xi^2$ for the triangular and $x_{c2}^2 = 2\pi\xi^2$ for the square vortex lattice. The maximum change occurs at $b \approx 0.15$ and $d \ge 4x_{c2}$. For thinner films and larger and smaller b, the variation of $\beta(z)$ is even smaller.

Thus, to a very good approximation, one may assume that the order parameter $\omega(x,y,z)$ of the vortex lattice inside films in perpendicular magnetic field is independent of z and for not too thin films has the same form as the 2D order parameter $\omega(x,y)$ of the bulk vortex lattice. For very thin films with $d \ll \xi$ at $b \ll 1$ the vortex cores are slightly wider than in the bulk. For example, at $b = 0.04$, $\kappa = 1.4$, the core width increases by about 25 % when d/ξ decreases from 0.5 to 0.005, but then saturates and does not increase further in thinner films. This is just the interval of d in which the modulation $1 - B_{\min}/B_{\max}$ of the periodic magnetic field $B(x,y,0)$ decreases from ≈ 1 to $\ll 1$ since the effective penetration depth $2\lambda^2/d$ becomes larger.

Close to B_{c2} the constancy along z of the GL function $\psi(x,y,z)$ applies to thicker and thicker films. This numerical result is consistent with the finding in Ref. 24 of a correlation length $l_z = \xi/(2\sqrt{1-b})$ that diverges for $b \to 1$ and describes the extension along the vortex lines of perturbations in $\psi(x,y,z)$ caused by small material inhomogeneities (pins). Interestingly, a similar diverging length $\xi/(2\sqrt{1-b})$ describes the long axis (along z) of a cigar-shaped superconducting region (nucleus) that nucleates at applied fields above B_{c2} at a small defect with transition temperature $T_c(\mathbf{r})$ higher than the bulk T_c.[19] In superconducting films of thickness $d < \xi|b-1|^{-1/2}$, or at applied fields satisfying $|B_a/B_{c2} - 1| < \xi^2/d^2$, small inclusions or precipitates are thus expected to cause a virtually 2D perturbation that has no z-dependence.

D. Surface energy

Next I consider the additional free energy caused by the presence of the two surfaces of the film. This energy per unit area of the film is composed of two terms:

(a) $F_{\rm stray}$, the magnetic energy of the stray field outside the film, defined by Eq. (9) and expressed in Eq. (13) in terms of the Fourier coefficients $b^s_{\mathbf{K}_\perp}$ of the field component $B_z(x,y,d/2)$ at the surface,

(b) $F_{\rm surf}$, the actual surface energy defined as the difference of the free energy of the film per unit area, $F_{\rm 3D}d$, minus the 2D bulk free energy density of the infinite vortex lattice, $F_{\rm 2D}$, times d, thus

$$F_{\rm surf} = (F_{\rm 3D} - F_{\rm 2D})d. \qquad (29)$$

The total surface energy, originating from both surfaces of the film, is the sum of these two terms, $F_{\rm stray} + F_{\rm surf}$. Both terms tend to a constant when the film thickness d increases above the vortex spacing x_1. These thick-film values of $F_{\rm stray}$ and $F_{\rm surf}$ are of the same order, and they are approximately equal for large $\kappa \gg 1$ and also at large reduced inductions $b \to 1$. This is so since the order parameter $\omega(x,y,z)$ in the film is nearly independent of z, and thus $F_{\rm surf}$ is virtually only of magnetic origin, i.e., it is the energy of the magnetic field change caused inside the film by the surface. When the magnetic penetration depth is large, $\lambda > x_1/2\pi \ll d$, this "inner stray field" is symmetric to the outer stray field. This equality applies also near $b = 1$, since inside the superconductor the magnetic screening is reduced by the reduction of the order parameter and thus the effective penetration depth $\lambda' = \lambda/\langle\omega\rangle^{1/2} \approx \lambda/(1-b)^{1/2}$ increases.[13]

The dependence of $F_{\rm stray}$ and $F_{\rm surf}$ on the film thickness is shown in Fig. 7 for $\kappa = 2$ and $b = 0.02$, 0.15, and 0.4. With increasing d both energies increase from zero and saturate to constant values at about $d/x_1 \ge 0.7$ for all κ and b. Figure 8 shows these thick-film limits of $F_{\rm stray}$ and $F_{\rm surf}$ as functions of the reduced induction b. Note that $F_{\rm stray}$ is slightly larger than $F_{\rm surf}$; this reflects the fact that the stray field inside the film is screened by $\lambda' < \infty$, while outside the film there is no screening ($\lambda = \infty$). Both $F_{\rm stray}$ and $F_{\rm surf}$ vanish at $b \to 0$ and at $b \to 1$ and have a maximum in between. At $b \to 0$ one has $F_{\rm stray} \approx F_{\rm surf} \propto b$ since each vortex contributes separately. At $b \to 1$ one has $F_{\rm stray} \approx F_{\rm surf} \propto (1-b)^2/\kappa$ (in units $\mu_0 H_c^2 \lambda$) since the amplitude of the periodic $B_z(x,y,d/2)$ decreases as $b^s_{\mathbf{K}_\perp} \propto (1-b)/\kappa$ and the depth of the stray field is $K_{10} \approx x_1/2\pi \propto \xi = \lambda/\kappa$. Therefore, when plotted in units $\mu_0 H_c^2 \xi$, all curves $F_{\rm stray}$ and all $F_{\rm surf}$ practically coincide for all $\kappa > 1$ and $b > 0.4$, see Fig. 8.

Note that the total surface energy $F_{\rm stray} + F_{\rm surf}$ is very small, never exceeding the value $8 \cdot 10^{-4} \mu_0 H_c^2 \xi$ reached at $\kappa \gg 1$ and $b \approx 0.2/\sqrt{\kappa}$.

E. Shear modulus of vortex lattice

Finally, the elastic shear modulus c_{66} of the vortex lattice will be discussed. As shown in Ref. 11, the shear modulus of the triangular vortex lattice can be expressed with high accuracy by the difference of the free energies of the rectangular lattice, $F_{\rm rect}$ (with $x_2 = 0$ and $y_2 = \sqrt{3}x_1/2$), and the triangular lattice, $F_{\rm tr}$ (with $x_2 = x_1/2$ and same $y_2 = \sqrt{3}x_1/2$),

$$c_{66} = (3\pi^2/2)(F_{\rm rect} - F_{\rm tr})\,. \qquad (30)$$

This is so since the free energy for constant unit cell height y_2 varies practically sinusoidally with x_2: $F(x_2) \approx F_{\rm tr} + [\,1 + \cos(2\pi x_2/x_1)\,](F_{\rm rect} - F_{\rm tr})/2$, thus the definition $c_{66} = \partial^2 F/\partial\alpha^2$ at small shear angle $\alpha = \arctan[(x_2 - 0.5)/y_2]$ yields Eq. (30).[25] Expressed in units $\mu_0 H_c^2$, the shear modulus depends on three variables: $c_{66} = c_{66}(b,\kappa,d)$. There are thus several ways to present the numerical data for c_{66}, each yielding different physical insight.

One result is that in the limit of small film thickness $d \ll \xi$ the shear modulus for a film with any κ tends to the bulk shear modulus at $\kappa \to \infty$, as already obtained by Conen and Schmid.[14] This finding may be understood from the fact that in thin films the vortices are Pearl vortices that have a long interaction range $2\lambda^2/d$ exceeding the London penetration depth λ.[4,5] This argument yields the correct limit $\kappa_{\rm eff} \to \infty$ for $d/\lambda \to 0$, but for $\kappa < \infty$ the c_{66} of films does not quantitatively coincide with the bulk c_{66} for an effective $\kappa_{\rm eff} = 2\lambda^2/d\xi = (2\lambda/d)\kappa \gg \kappa$, since c_{66} is determined not only by the range but by the full shape of the interaction potential between vortices, which differs for Abrikosov[1] and Pearl[4] vortices. If this

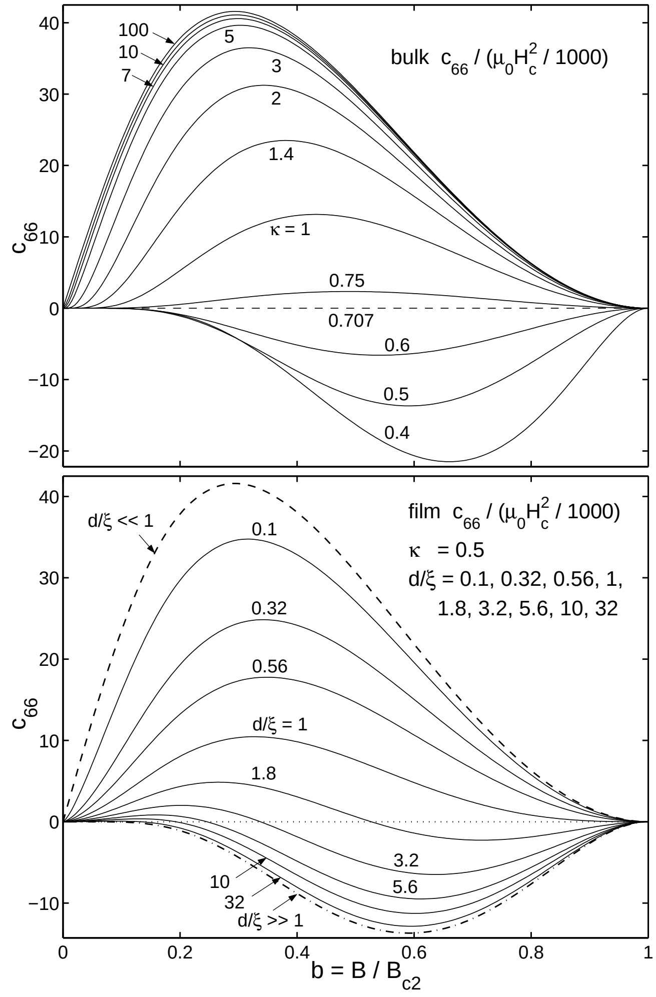

FIG. 9: Top: The shear modulus c_{66} of the bulk ($d \to \infty$) triangular vortex lattice as function of the reduced induction $b = \bar{B}/B_{c2}$ for GL parameters $\kappa = 0.4$, 0.5, 0.6, .707, 0.75, 1, 1.4, 2, 3, 5, 7, 10, 100, in units $\mu_0 H_c^2/1000$. For $\kappa < 2^{-1/2} = 0.707$ one has formally $c_{66} < 0$, though vortices and a vortex lattice are unstable in such type-I superconductors. Bottom: The shear modulus c_{66} of the triangular vortex lattice in films with thicknesses $d/\xi = 0.1$, 0.32, 0.56, 1, 1.8, 3.2, 5.6, 10, and 32, plotted versus b for $\kappa = 0.5$. This c_{66} is positive, i.e. the triangular vortex lattice is stable, for sufficiently thin films or small inductions. For $d \gg \xi$ the bulk c_{66} at the same $\kappa = 0.5$ is reached (dash-dotted line), and for $d \ll \xi$ the bulk c_{66} in the limit $\kappa \gg 1$ (dashed line).

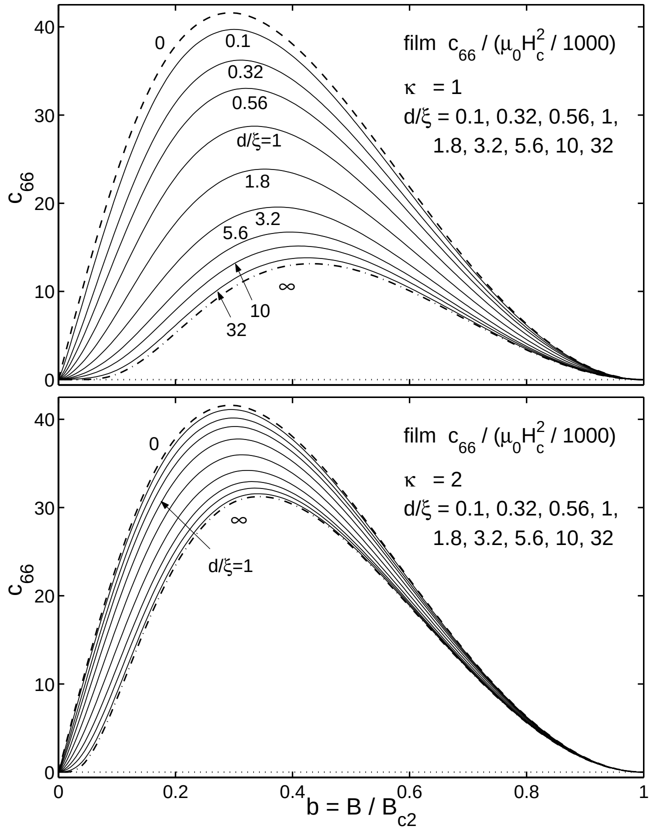

FIG. 10: The shear modulus c_{66} of the triangular vortex lattice in films of various thicknesses like in Fig. 9 bottom, but for $\kappa = 1$ (top) and $\kappa = 2$ (bottom), in units $\mu_0 H_c^2/1000$.

potential is $V(r)$ with $r = (x^2 + y^2)^{1/2}$ and the vortex density is $n_v = \bar{B}/\Phi_0$, one has for a 2D triangular lattice with positions $\mathbf{R}_{mn}$ defined below Eq. (3):[26,27]

$$c_{66} = \frac{n_v}{16} \sum_{m,n} \left[R_{mn}^2 V''(R_{mn}) + 3 R_{mn} V'(R_{mn}) \right], \qquad (31)$$

see also Eqs. (9) and (11) of Ref. 28.

Figures 9 and 10 show c_{66} as a function of the reduced induction b for different film thicknesses d expressed in units of the GL coherence length ξ, $d/\xi = 10^{(-4,\ldots,6)/4} = 0.1, \ldots, 32$, and for GL parameters $\kappa = 0.5$, 1, and 2. For large $\kappa \geq 5$, the curves $c_{66}(b)$ for various thicknesses are very close to each other and to the bulk c_{66}. In general, the curves for finite film thickness all fall between the two limiting cases $d \to \infty$ coinciding with the bulk $c_{66}(\kappa)$, and $d \to 0$ coinciding with the bulk $c_{66}(\kappa = \infty)$. This interval is very small for large κ and not too small b since $c_{66}(\kappa = \infty) - c_{66}(\kappa) \propto \kappa^{-2}$. This means that for large $\kappa \geq 5$ the shear modulus is nearly the same for thin and thick films. Note that for the bulk and $\kappa \geq 5$ one has $c_{66} \approx B\Phi_0/(16\pi\mu_0\lambda^2) \propto b$ for $1/(2\kappa^2) \leq b \leq 0.15$ (see Fig. 9 top); this applies also to films. For $\kappa \leq 5$ we confirm the finding of Ref.[14] that $c_{66} \propto b^{3/2}$ for $b \ll 1$, but this law applies only to intermediate film thicknesses $0.5 \leq d/\lambda \leq 3$ at $b \leq 0.1$.

An interesting feature can be seen from Fig. 9. The upper part shows the *bulk* $c_{66}(b, \kappa)$ for values $\kappa = 0.4$ to ∞, i.e., also for $\kappa < 1/\sqrt{2} = 0.707$ corresponding to type-I superconductors, in which the vortex lattice is energetically unfavorable in the bulk. For $\kappa < 0.707$ one finds *negative* $c_{66} < 0$. This means the bulk rectangular and square vortex lattices[25] have lower energy than the triangular lattice (the Meissner state without vortices has

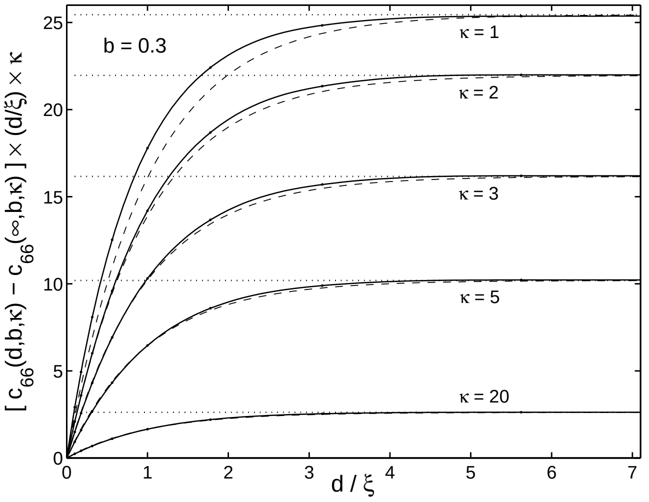

FIG. 11: Dependence of the shear modulus c_{66} of the triangular lattice on the film thickness d. Plotted is the additional rigidity caused by the film surfaces in form of $f(d,b,\kappa) = [\,c_{66}(d,b,\kappa) - c_{66}(\infty,b,\kappa)\,] \cdot (d/\xi) \cdot \kappa$ versus d at $b = 0.3$ for various $\kappa = 1 \ldots 20$ (solid lines, c_{66} in units $\mu_0 H_c^2/1000$). The dashed lines show the fit, Eq. (32), with $l = \xi$.

even lower energy in this case). However, as can be seen in the lower plot for films with $\kappa = 0.5$, in sufficiently thin type-I superconductor films the triangular vortex lattice can be stable (i.e., $c_{66} > 0$) when the induction is sufficiently small. This behavior was seen also in Ref. 14.

The dependence of c_{66} on the film thickness d is visualized in Fig. 11 by plotting the difference

$$f(d,b,\kappa) = [\,c_{66}(d,b,\kappa) - c_{66}(\infty,b,\kappa)\,] \cdot (d/\xi) \cdot \kappa \qquad (32)$$

(an energy per unit area) versus d at various κ values for $b = 0.3$ (near the maximum of c_{66}). One can see that this function saturates when the film thickness exceeds a few coherence lengths ξ. For all values of κ and $b > 1/\kappa^2$ one can fit these curves closely by

$$f(d) \approx f(\infty)[\,1 - \exp(-d/l)\,]\,. \qquad (33)$$

In Fig. 11 (at $b = 0.3$) the length l of the best fit accidentally coincides with ξ, but in general l depends on b and is proportional to the vortex spacing x_1: $l \approx 0.195 x_1 = (\sqrt{6}/4\pi) x_1 = \sqrt{2}/K_{10}$, thus $l/\xi \approx 3^{1/4}(2\pi)^{-1/2}/\sqrt{b} = 0.525/\sqrt{b}$, yielding $l = 0.96\xi$ at $b = 0.3$. This saturation means that the additional rigidity of the vortex lattice caused by the film surfaces and measured by $f(d,b,\kappa)$, becomes independent of d in films thicker than a few coherence lengths, and thus one has $c_{66}(d) - c_{66}(\infty) \propto 1/d$. For thin films with $d \ll \xi$ one has $f(d,b,\kappa) \propto d$ since $c_{66}(d) - c_{66}(\infty)$ is a constant independent of d.

Figure 12 visualizes the κ dependence of the shear modulus of the triangular lattice by plotting $[\,c_{66}(\infty,b,\infty) - c_{66}(d,b,\kappa)\,] \cdot \kappa^2$ versus $1/\kappa$ at $b = 0.1$, 0.3, and 0.7, for film thicknesses $d/\xi = 0.1 \ldots 10$. Also shown are the limits $d = 0$ (the x-axis), proving that $c_{66}(d \to 0, b, \kappa) = c_{66}(d \to \infty, b, \kappa \to \infty)$ for any κ, and $d = \infty$ (upper dashed line) that coincides with $[\,c_{66}^{\rm bulk}(\kappa = \infty) - c_{66}^{\rm bulk}(\kappa)\,] \cdot \kappa^2$. These plots prove that the differences of any two c_{66} values vanish as κ^{-2} when $\kappa \to \infty$. One can see that this asymptotic law is a good approximation even for not so large $\kappa \geq 2$, and at large $b \geq 0.7$ it practically applies to all $\kappa \geq 0.71$, and even for type-I superconductors with not too small $\kappa < 0.71$.

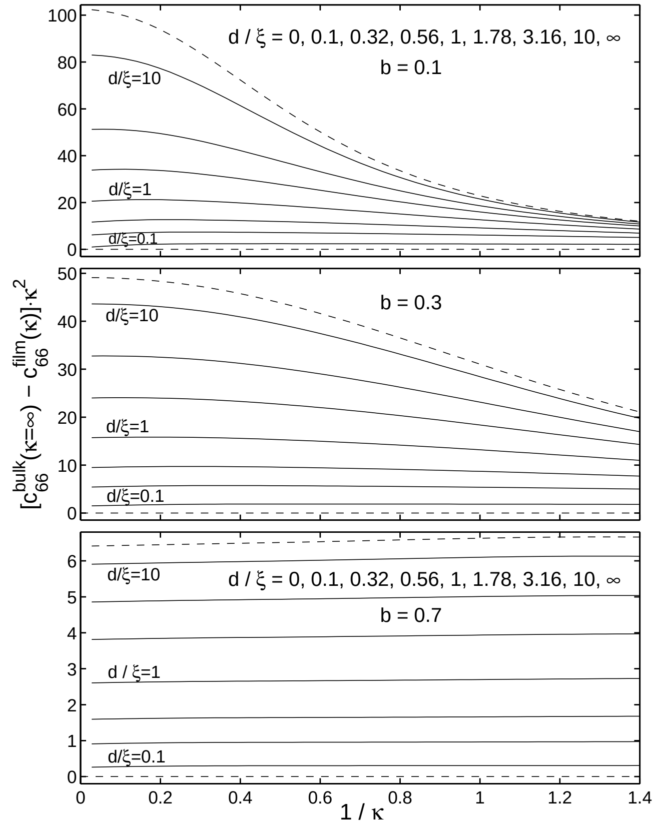

FIG. 12: Dependence of the shear modulus c_{66} of the triangular lattice on the GL parameter κ. Plotted is the function $[\,c_{66}(\infty,b,\infty) - c_{66}(d,b,\kappa)\,] \cdot \kappa^2$ versus $1/\kappa$ at $b = 0.1$ (top), 0.3 (middle), and 0.7 (bottom), for various film thicknesses d/ξ (c_{66} in units $\mu_0 H_c^2/1000$). The dashed lines show the limits $d = 0$ (x-axis) and $d = \infty$ (upper line) coinciding with $[\,c_{66}^{\rm bulk}(\kappa = \infty) - c_{66}^{\rm bulk}(\kappa)\,] \cdot \kappa^2$. It is clearly seen that the differences of any two c_{66} values vanish as κ^{-2} when $\kappa \to \infty$. This asymptotic law is good even for $\kappa \geq 2$, and it practically applies to all $\kappa \geq 0.71$ at large inductions $b \geq 0.7$.

In Fig. 13 the numerical $c_{66}(d,b,\kappa)$ is compared with the analytical result of Conen and Schmid, Fig. 1 of Ref. 14, valid at large inductions $1 - b \ll 1$. Their result was obtained from an elegant expression derived by Lasher[18] for the free energy of films with vortex lattice of arbitrary symmetry at $b \to 1$. Lasher[18] implicitly used the fact that the magnetic stray field inside the film is not screened in this limit of $b \to 1$.

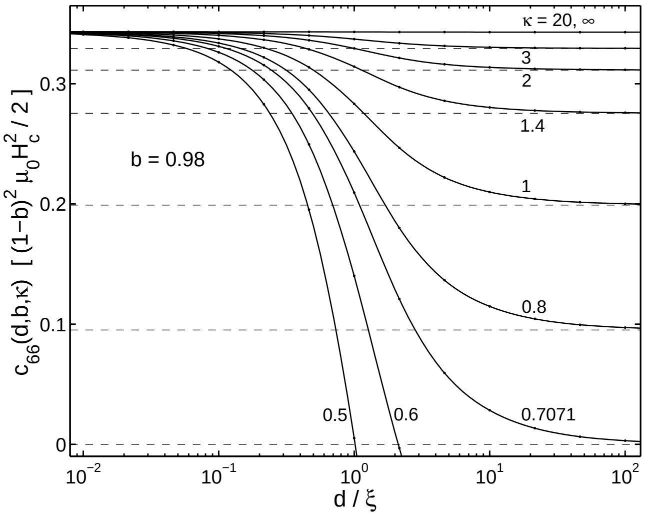

FIG. 13: The shear modulus $c_{66} \propto (1-b)^2$ of the vortex lattice in films at high inductions $1-b \ll 1$, plotted versus the film thickness d. For comparison with Fig. 1 of Ref. 14, c_{66} is in the same units $(1-b)^2 \mu_0 H_c^2/2$. The horizontal dashed lines denote the bulk c_{66}. This plot, computed for $b = 0.98$, applies approximately too all $b \geq 0.6$ and agrees with the analytic expression plotted in Fig. 1 of Ref. 14.

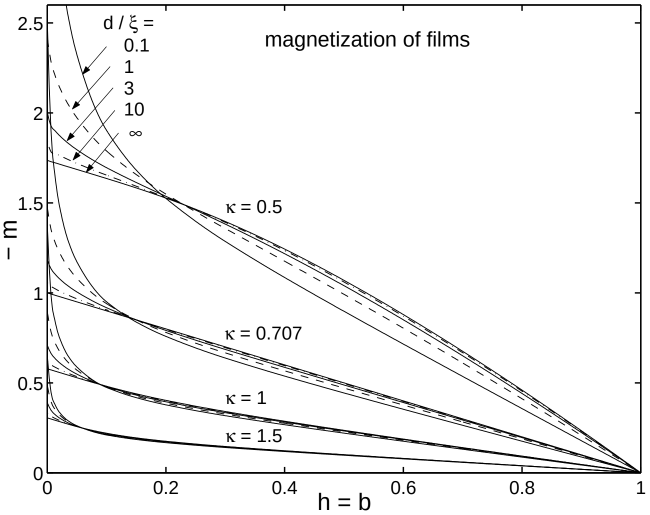

FIG. 14: The magnetization of infinite films with thickness $d/\xi = 0.1$, 1 ,3, 10, ∞, containing a triangular vortex lattice with one flux quantum per vortex. Plotted is $-m = -M/H_{c2}$ versus $h = H/H_{c2} = b = B/B_{c2}$ for $\kappa = 0.5$, 0.707, 1, 1.5.

F. Magnetization of infinite films

For infinitely extended films the average magnetic induction $\bar{B}$ equals the applied field, $\bar{B} = \mu_0 H_a$, and the magnetization M is defined as the magnetic moment per unit volume of the film. The demagnetization factor of infinite films is $N = 1$, and thus the effective lower critical field at which the first vortices penetrate is $H'_{c1} = (1-N)H_{c1} = 0$. For the magnetization of superconductors with general demagnetizing factor $0 \leq N \leq 1$ see, e.g., Refs. 19,29. Noting that the total free energy per volume $F_{\rm tot}$, Eq. (9), equals the work done by the applied field, which may be written as $-\int M\, dB$, one obtains the relation $M = -\partial F_{\rm tot}/\partial B$. Figure 14 shows magnetization curves for films of various thicknesses d/ξ = 0.1, 1, 3, 10, and ∞ for GL parameters $\kappa = 0.5$, $1/\sqrt{2}$, 1, and 1.5.

For thick films ($d \gg \xi, \lambda$) at $\kappa = 1/\sqrt{2}$ one has $F_{\rm tot} = -\frac{1}{2}(1-b)^2$ and thus $-m = 1-b = 1-h$; for larger $\kappa > 0.707$ the thick film $-m(h)$ is concave (has positive curvature); and for smaller $\kappa < 0.707$ (type I superconductors) $-m(h)$ is convex (has negative curvature) and the vortex lattice is not stable. However, for sufficiently thin films, even when $\kappa < 0.707$ the curvature of $-m(h)$ can be positive and even may change sign at a certain value of $h = b$. Note that the plotted curves $-m(h)$ for various d/ξ cut each other approximately at $h = b \approx 1/\kappa$. For thick films the initial slope is $-m'(h)|_{h=0} = -1$ for all κ, and $-m(0) = h_{c1} = H_{c1}/H_{c2}$. This is so since when surface contributions may be disregarded, one has for superconducting ellipsoids $-M = H_{c1}$ at $H = H'_{c1}$ where $B = 0$. The enhancement of $-m(h)$ at small $h < \kappa$ for thin films in Fig. 14, originates from the energy of the magnetic stray field, which enhances the self energy of a vortex beyond its bulk value $d\Phi_0 H_{c1}$. More details about this will be published elsewhere.

IV. SUMMARY

It is shown how the Ginzburg-Landau equations can be solved for a periodic lattice of Abrikosov vortices in superconducting films in a perpendicular magnetic field. As illustration how well this iteration method works, some results are presented. The widening of the magnetic field lines as they exit the film surface is correctly obtained, Figs. 1, 2, but this leads only to a very small correction of the order parameter near the surface, Fig. 1. The variance of the transverse component of the magnetic induction is sharply peaked at the surface and vanishes deep inside and far outside the film, Figs. 4, 5. The variance of the periodic order parameter (Abrikosov parameter β) varies very little across the film thickness, by at most a factor 1.0033, Fig. 6. The surface energy saturates for large film thickness d and vanishes linearly at small d, Fig. 7. For not too thin films the surface energy originates mainly from the magnetic stray field, which comes in approximately equal parts from outside and inside the film, in particular for large κ or large b, Fig. 8. For very thin films the stray field energy may be disregarded and the very small surface energy comes mainly from the small modification of the order parameter, Fig. 7. The shear modulus $c_{66}(d, b, \kappa)$ of the triangular vortex lattice in thin films approaches the $c_{66}(\infty, b, \infty)$ of thick films (bulk limit) at $\kappa \to \infty$, Fig. 10, the difference being proportional to κ^{-2}, Fig. 12. While the bulk $c_{66}(\infty, b, \kappa)$ is negative in type-I superconductors ($\kappa < 0.707$), the c_{66} of sufficiently thin films can be positive and may change sign at some value of b, Fig. 9. The magnetization curves of films with $\kappa < 0.707$ may have positive or negative curvature, depending on the film thickness, Fig. 14. More results will be published elsewhere. Extensions of this method to vortices with several flux quanta and to the periodic lattice of curved vortices in superconducting films in a tilted magnetic field are underway.

APPENDIX A: PRESENTATION OF FIELD LINES

A practical question is how to plot the magnetic field lines of this 3D problem such that they have the correct orientation of $\mathbf{B}(x, y, z)$ and their 1D density (reciprocal distance) in the plotted plane is proportional to the magnitude $|\mathbf{B}(x, y, z)|$. A simple consideration shows that this is possible only for 2D planar problems, when the field lines coincide with the contour lines of the vector potential, e.g., $A_y(x, 0, z)$. But for 3D magnetic fields, and even for cylindrically symmetric fields, such 2D plots of the field lines are not possible since the magnitude $|\mathbf{B}(x, y, z)|$ here is proportional to the 2D density of the 3D field lines, but not to the 1D density of the plotted 2D field lines. For our 3D problem of a thick film with a 2D periodic vortex lattice we have two possibilities to plot field lines that approximately have the above mentioned properties.

First method: One may use numerical programs that plot the field lines (stream lines) of the 2D planar field $\mathbf{B}(x, 0, z) = (B_x, B_z)$ [or any other planar cross section of $\mathbf{B}(x, y, z)$] starting from equidistant points ($x = x_i, y = 0, z = -z_0$) far away from the film surface so that $\mathbf{B}(x, y, z) \approx \bar{B}\hat{\mathbf{z}} = \text{const}$. Such field lines have the correct slope, but their density is only approximately proportional to $|\mathbf{B}(x, y, z)|$.

Second method: In this paper the 2D plots of the magnetic field lines show the contour lines of the function

$$\varphi(x, z) = \int_0^x B_z(x, 0, z)\, dx \Big/ \int_0^{x_1} B_z(x, 0, z)\, dx\,, \quad \text{(A1)}$$

which ranges from $\varphi(0, z) = 0$ at $x = 0$ (vortex center) to $\varphi(x_1/2, z) = 1$ (middle plane between two vortices) and has a periodic derivative. Such field lines have a 1D density along x proportional to $|B_z(x, 0, z)|$, and a density perpendicular to these lines which is close to $|\mathbf{B}(x, y, z)|$, since their orientation is close to the orientation of $\mathbf{B}(x, y, z)$. Figure 2 shows that these two types of field lines are very similar. In particular, the contour lines of $\varphi(x, z)$, Eq. (1), have slopes that are close to the correct slope.

---

[1] A. A. Abrikosov, Zh. Eksp. Teor. Fiz. **32**, 1442 (1957) [Sov. Phys. JETP **5**, 1174 (1957)].

[2] P. G. DeGennes, *Superconductivity of Metals and Alloys* (New York, Benjamin, 1966).

[3] M. Tinkham, Introduction to Superconductivity (McGraw-Hill: New York 1975).

[4] J. Pearl, Appl. Phys. Lett. **5**, 65 (1964).

[5] J. R. Clem, Phys. Rev. B **43**, 7837 (1991).

[6] O. Fritz, M. Wülfert, H. J. Hug, H. Thomas, and H.-J. Güntherodt, Phys. Rev. B **47**, 384 (1993).

[7] D. Yu. Irz, V. N. Ryzhov, and E. E. Tareyeva, Phys. Lett. A **207**, 374 (1995).

[8] J.-C. Wei and T.-J. Yang, Jpn. J. Appl. Phys. **35**, 5696 (1996).

[9] G. Carneiro and E. H. Brandt, Phys. Rev. B **61**, 6370 (2000).

[10] E. H. Brandt, phys. stat. sol. (b) **51**, 345 (1972).

[11] E. H. Brandt, Phys. Rev. Lett. **78**, 2208 (1997).

[12] E. H. Brandt, Phys. Rev. B **68**, 054506 (2003).

[13] E. H. Brandt, Rep. Prog. Phys. **58**, 1465 (1995). In Eqs. (1.4), (1.7), and (1.8) of that paper the wrong denominator $(2\kappa^2 - 1)\beta_A$ has to be replaced by $1 + (2\kappa^2 - 1)\beta_A = 2\beta_A(\kappa^2 - 0.069)$.

[14] E. Conen and A. Schmid, J. Low Temp. Phys. **17**, 331 (1974).

[15] M. Tinkham, Phys. Rev. **129**, 2413 (1963).

[16] M. Tinkham, Rev. Mod. Phys. **36**, 268 (1964).

[17] K. Maki, Ann. Phys. (N.Y.) **34**, 363 (1965).

[18] G. Lasher, Phys. Rev. **154**, 345 (1967).

[19] A. Fetter and P. C. Hohenberg, Phys. Rev. **159**, 330 (1967).

[20] R. A. Klemm and J. R. Clem, Phys. Rev. B **21**, 1868 (1980).

[21] V. G. Kogan and J. R. Clem, Phys. Rev. B **24**, 2497 (1981).

[22] R. A. Klemm, Phys. Rev. B **38**, 6641 (1988).

[23] J. R. Kirtley, V. G. Kogan, J. R. Clem, and K. A. Moler, Phys. Rev. B **59**, 4343 (1999).

[24] E. H. Brandt, phys. stat. sol. (b) **71**, 277 (1975).

[25] In Eq. (5) of Ref. 12 erroneously $F_{\rm sq}$ (square lattice) was written in place of $F_{\rm rect}$. This form of Eq. (30) becomes numerically correct if the factor $(3\pi^2/2) = 14.8$ is replaced by 23.1, i.e., $F_{\rm sq}$ lies approximately in the middle between $F_{\rm tr}$ and $F_{\rm rect}$.

[26] R. Labusch, phys. stat. sol. **19**, 715 (1967).

[27] E. H. Brandt, phys. stat. sol. **35**, 1027 (1969).

[28] E. H. Brandt, J. Low Temp. Phys. **26**, 735 (1977).

[29] E. H. Brandt, Phys. Rev. B **60**, 11939 (1999).